

Numerical Simulation of the Response of General Circulation of the Middle Atmosphere to Spatial Inhomogeneities of Orographic Waves

N. M. Gavrilov^a, A. V. Koval'^a, A. I. Pogorel'tsev^b, and E. N. Savenkova^b

^a St. Petersburg State University, ul. Ul'yanovskaya 1, St. Petersburg, 198504 Russia

^b Russian State Hydrometeorological Institute, Malookhtinskii pr. 98, St. Petersburg, 195106 Russia

e-mail: gavrilov@pobox.spbu.ru; koval_spbu@mail.ru

Received April 13, 2012; in final form, October 23, 2012

Abstract—We have developed a parameterization of the dynamical and thermal effects of stationary orographic waves (SOWs) generated by the earth's surface topography and included it into the general circulation model of the middle and upper atmosphere. We have analyzed the sensitivity of atmospheric general circulation at tropospheric to thermospheric altitudes to the impact of SOWs propagating from the troposphere. Changes in atmospheric circulation due to variations in the SOW generation and propagation have been considered for different seasons. It has been shown that, during solstices, the main dynamical and thermal impacts the middle atmosphere of winter hemispheres, where the SOW-induced changes in the velocity of zonal circulation can reach 30%. During equinoxes, the SOW impact is distributed more homogeneously between the Northern and Southern hemispheres, and the relative changes in the velocity of zonal circulation of the middle atmosphere may constitute 10%.

Keywords: atmospheric circulation, mesoscale waves, orography, wave acceleration, heat influx, parameterization

DOI: 10.1134/S0001433813040038

1. INTRODUCTION

Recent numerical simulations of the general circulation of the middle and upper atmospheres have increased interest in the study of accelerations of the mean flow and heat influxes generated by dissipating internal waves in the atmosphere. A key source of these waves is the topography of the earth's surface. The orographic waves produced by the interaction of the earth's surface (which is inhomogeneous by height) with incident atmospheric flow can propagate into the middle atmosphere and create significant accelerations of the mean flow and heat influxes, which can affect the general circulation and thermal conditions of the atmosphere. There are simplified algorithms for parameterizing the thermal and dynamical effects of orographic waves (for example, [1–3]) incorporated into numerical models. The calculation of wave accelerations of the mean flow and heat influxes by these parameterizations ignores atmospheric rotation, which can significantly affect the parameters of stationary orographic waves (SOWs) with frequencies $\sigma = 0$.

The orography and jet streams are known to be nonuniformly distributed over the globe and prone to seasonal variations [4], which lead to differences in wave characteristics in the winter and summer hemi-

spheres. Satellite measurements of mesoscale variations in self-radiation, temperature, and refractive index of the atmosphere [5–8] have shown considerable inhomogeneity of latitude–longitude distributions of orographic wave characteristics in the troposphere and stratosphere, which are highly dependent on the season. Therefore, it is of current interest to incorporate the observed nonuniform distributions of wave sources into numerical models of the general circulation of the middle atmosphere.

In this study, the parameterization of dynamic and thermal effects of the SOWs developed by the authors [9] has been incorporated into a numerical model of the general circulation of the middle and upper atmosphere. The sensitivity of atmospheric general circulation to the SOW effects from tropospheric to thermospheric altitudes has been analyzed. The changes in atmospheric circulation under variable conditions of SOW generation have been considered for different seasons.

2. PARAMETERIZATION OF SOW EFFECTS

The used parameterization of dynamic and thermal effects of SOWs in the atmosphere was described in [9]. The total vertical flux of wave energy and the amplitude of horizontal velocity oscillations were cal-

culated from the polarization relations for SOWs taking into account the atmospheric rotation and obtained in [9]. These relationships were used to derive a differential equation describing the change in the SOW amplitude with height. This equation is solved for a given wave amplitude at the lower boundary and given altitude profiles of the mean wind and temperature. Then these formulas are used to calculate the wave acceleration and total heat influx, which can be used in atmospheric dynamical models (see [9]).

In this study mesoscale orography is parameterized using a modification of the subgrid-scale orography scheme [3] with horizontal scales of the orographic height change smaller than the horizontal grid interval of the numerical model. In our parameterization [9], the scales of subgrid topography height variations from 20 to 200 km [3] are numerically filtered by averaging over segments of the earth's surface with Gaussian weighting functions. In the neighborhood of each node of the horizontal grid of the model, the subgrid-scale terrain is approximated by an effective ellipse [1]. The use of forces acting on the incident atmospheric flow from the effective elliptical mountain barrier with the help of methods [10] makes it possible to determine the amplitude and effective horizontal wave number of SOW at the lower boundary, which are necessary for the above-described calculations (see [9]). This study uses the ETOPO2 global 2-min (along latitude and longitude) database of the earth's surface elevations.

3. NUMERICAL MODEL OF THE GENERAL CIRCULATION OF THE ATMOSPHERE

To study the effect of SOWs on the atmospheric dynamics, we have incorporated the parameterization described above into the numerical model of the general circulation of the middle and upper atmosphere (MCMUA) [11, 12], which was developed on the basis of the Cologne Model of the Middle Atmosphere—Leipzig Institute for Meteorology (COMMA-LIM) [13]. The basis of these modifications is the model developed earlier in the University of Cologne, Germany [14]. A brief description of its equations and main physical processes can be found in [15]. The model is based on the standard system of primitive equations in spherical coordinates. The model takes into account the processes of radiative heating and cooling of the atmosphere due to gas constituents O, O₂, O₃, H₂O, CO₂, and NO. At lower thermospheric heights, additional dynamical sources of heat are used. The model incorporates ion drag, molecular viscosity, heat conduction, and turbulent diffusion. The model allows excitation of planetary waves near the earth's surface and a change in the surface albedo.

The calculations were performed for altitudes from 0 to 150 km; however, the weather changes and clouds in the troposphere are not modeled. The basic parameters calculated by the model are zonal, meridional,

and vertical velocity components; geopotential; and temperature. The Marchuk–Strang splitting scheme [16, 17] and the Matsuno scheme (for time integration) [18] are used. The solution stability is secured by a Fourier filter that limits the zonal resolution to 500 km. The horizontal grid intervals of the model are 5.6° in longitude and 5° in latitude in the range from 87.5° S to 87.5° N. The vertical grid interval is constant in the coordinate $z = H \ln(p_0/p)$, where p_0 is the surface pressure and $H = 7$ km. These calculations were performed using a version of the model with 48 vertical levels and a vertical step of around 2.7 km. The time integration step is 450 s.

The lower boundary conditions are the seasonal-mean climatic distributions of geopotential height and temperature given at the isobaric level of 1000 hPa. The prognostic equation for temperature contains an additional term proportional to the difference between calculated and observed seasonal-mean temperatures in the stratosphere by the UK Met Office data. The constant of proportionality is inversely proportional to characteristic time (~5 days) of relaxation of the calculated temperature to the observed one. This makes it possible to realistically reproduce the location and intensity of jet streams in the troposphere.

Because the SOW amplitudes in the surface layer are small, the calculation of wave characteristics with the parameterization scheme described in Section 2 starts from an altitude of 7 km, to which the surface values of SOW characteristics are extrapolated. The calculated heat influxes generated by SOWs are added to the heat-influx equation in MCMUA, and the zonal and meridional components of wave acceleration are added to the MCMUA equation for the corresponding velocity components.

The initial approximation is a windless stratified atmosphere with a realistic vertical profile of temperature. The first 150 days of model calculations involve several stages of “adaptation.” In the first 30 days, the calculations are performed with constant values of geopotential height at the lower boundary; starting from the 31st day, the observed changes are introduced. In the first 120 days, the calculations are based on only the daily average heating of the atmosphere; then the diurnal variations of heating are gradually taken into account and an additional prognostic equation is used for the geopotential at the lower boundary. Until day 150, the model calculations are performed for a fixed position of the earth on the orbit; then the model takes into account the seasonal change in solar heating. The initial dates of calculations are chosen so that the model days from 151 to 210 correspond to January–February, April–May, July–August, and October–November.

4. RESULTS OF CALCULATIONS

To study the effect of orographic waves generated by the earth's surface topography and propagating

upward to the general circulation and the thermal regime of the middle atmosphere, we performed calculations using the MCMUA model (described in Section 3) with the parameterization of dynamical and thermal effects of SOWs (see Section 2). The calculations were performed for conditions corresponding to different seasons. For each set of initial data, we calculated the hydrodynamic fields (wind speed, temperature, geopotential, etc.) with and without the effects of SOWs. The differences between corresponding hydrodynamic variables in these calculations show the increment in velocity (IV), increment in temperature (IT), and increment in geopotential (IG) caused by the dynamical and thermal effects of SOWs in the middle atmosphere. Positive or negative values of IV, IT, and IG mean an increase or decrease in the respective hydrodynamic variables when the effect of SOWs is taken into account.

Seasonal-mean distribution. Figure 1a shows the zonal wind (averaged for January and over longitude) calculated with the MCMUA model. It can be seen from Fig. 1 that the tropospheres of the Northern (winter) and Southern (summer) hemispheres have eastward jet streams with velocity peaks of around 30 m/s at latitudes from 30°–50° in both hemispheres. In the winter stratosphere of the Northern hemisphere, the zonal flow keeps its direction unchanged and the jet-stream velocity increases up to 80–90 m/s at altitudes of around 60 km and at latitudes of 50°–60° N. In Fig. 1a, the wind direction in the strato-mesosphere of the summer (Southern) hemisphere is reversed and an eastward jet stream is generated with a maximum velocity at altitudes of 50 to 70 km. In the altitude range from 90 to 110 km, the circulation in both hemispheres is reversed westward in the winter (Northern) hemisphere and eastward in the summer (Southern) hemisphere. These specific features of the circulation of the middle atmosphere are well known and related with altitude–latitude features of heat influxes in the middle atmosphere [19]. The structure of the zonal circulation presented in Fig. 1a, as well as the temperature fields calculated by the MCMUA model, is in a rather good agreement with the CIRA-86 and MSISE-90 empirical standard models.

The zonal circulation inhomogeneities shown in Fig. 1a affect the distribution of orographic waves. This can be seen in Fig. 1b, which shows the zonal-mean amplitude of SOW velocity oscillations for January. In the summer strato-mesosphere of the Southern hemisphere near critical levels, where the zonal flow velocity vanishes, a strong turbulent viscous attenuation of SOWs occurs due to a sharp decrease in their vertical lengths. This creates an effective barrier to the penetration of SOWs; therefore, the wave amplitudes in middle and high latitudes of the summer (Southern) hemisphere above 20 km are reduced (Fig. 1b). At low-latitudes of the summer (Southern) hemisphere and in the winter (Northern) hemisphere, the SOW amplitudes have significant values up to greater

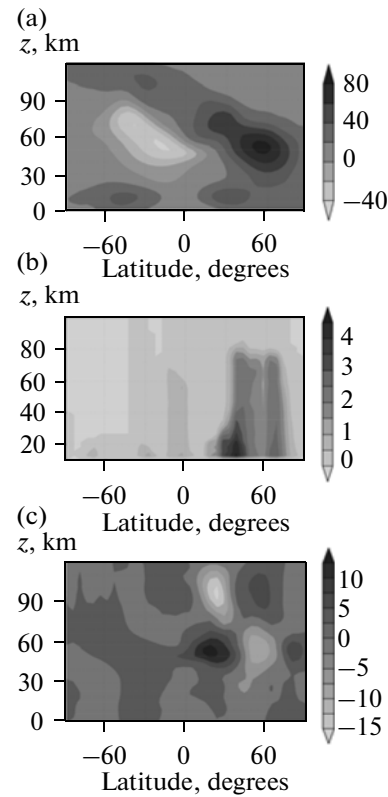


Fig. 1. Calculated by the model for average January (a) zonal-mean wind velocity in m/s, (b) amplitude of oscillations in SOW velocity in m/s, and (c) incremental velocity (IV) of zonal circulation (m/s) due to the impact of SOWs.

heights (Fig. 1b). In [9], the vertical profiles of the SOW amplitude were shown to depend on the profiles of average wind, temperature, molecular and turbulent viscosity, and heat conduction. Under low dissipation in the lower atmosphere, the SOW amplitudes can quasi-exponentially grow with height. At high altitudes, the growing kinematic molecular and turbulent viscosity and heat conduction can lead to the attenuation of SOWs with sufficiently small vertical lengths. In addition, the SOW amplitudes depend on the position of mountain systems, which are found more in mid-latitudes of the Northern Hemisphere than in the Southern Hemisphere [9].

The combination of these factors leads to significant values of SOW amplitudes at mid-latitudes of the winter (Northern) hemisphere up to heights of 80–90 km (see Fig. 1b). Similar results on the prevalence of SOW amplitudes in the middle atmosphere of the winter hemisphere were obtained by numerical simulation [20]. An increase in the amplitude of mesoscale waves in the strato-mesosphere of the winter hemisphere was recorded in many experiments (for example, see the seasonal variations in the amplitude of mesoscale waves at heights of 20–40 km from data of SABER and AIRS infrared middle-atmospheric sounding instruments and TIMED and Aqua satellites, respectively

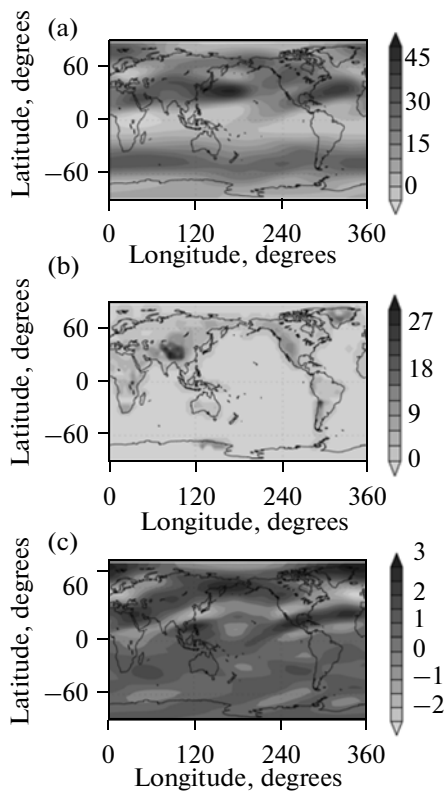


Fig. 2. (a) Latitude–longitude distributions of zonal wind velocity at an altitude of 7 km in m/s, (b) incremental velocity (IV) of zonal wind due to the impact of SOWs at an altitude of 12 km in m/s, and (c) amplitude of SOW velocity at an altitude of 12 km in m/s for January.

[21, 22], as well from data of an analysis of measurements on the CHAMP GPS satellite [8]).

The calculations of the seasonal-mean altitude–latitude structure of SOW amplitudes for other seasons indicated that in July, the Northern and Southern hemispheres are reversed when compared with Fig. 1b. The strato-mesosphere of the Northern (now summer) hemisphere has an emerging westward jet stream, which leads to filtered SOWs at critical levels. In the winter (Southern) hemisphere in July, the SOWs can propagate to greater heights; here, their amplitudes on average are smaller than those in the Northern hemisphere in January due to a smaller number of mountain systems in the Southern Hemisphere than in the Northern Hemisphere.

The strato-mesosphere in the spring and fall is characterized by a restructured circulation, when the westward jet streams are destroyed and affect SOW filtering less. Therefore, the SOW amplitudes in the middle atmosphere during the equinoxes are more uniformly distributed between Southern and Northern hemispheres.

Figure 1c shows the altitude–latitude structure of seasonal-mean increments in wind velocity in January on account of the SOW effect (see above). It can be

seen that the changes in the circulation velocity peak at mid-latitudes of the winter (Northern) hemisphere, where the areas of maximum SOW amplitudes are located (see Fig. 1c). Here, at altitudes of 30–70 km in the Northern Hemisphere, there are alternating areas of positive (to 20 m/s) and negative (to –15 m/s) IVs. Due to the SOW effect in these areas, the zonal circulation of the middle atmosphere, which is eastward in winter, becomes intensified or weakened, respectively. Figure 1c also shows areas of negative (to –20 m/s) and positive (to 5 m/s) IVs in the Northern Hemisphere at altitudes of 70–120 km. In the middle atmosphere of the summer (Southern), positive IVs of up to 5 m/s are observed in low- and mid-latitudes (Fig. 1c).

The results of similar calculations for July show that the SOW effect on the zonal circulation in the winter (now Southern) hemisphere is still the highest. This largely involves a strengthened eastward zonal-mean circulation (positive IVs) at altitudes of 80–90 km and at latitudes of 50°–60° S and in the stratosphere near 30° S, as well as a weakened circulation (negative IVs) at latitudes of 20°–30° S and altitudes of 80–90 km. In addition, we estimated the effect of SOWs on the general circulation of the atmosphere during the equinoxes. In April at altitudes of around 70 km, the zonal circulation is decreased at 60°–70° S and the velocity is increased at 50°–60° S; the zonal circulation velocity also varies at low-latitudes of the Northern Hemisphere. In October, the seasonal-mean circulation velocity changes up to 10%, mainly at high-latitudes of the Northern Hemisphere.

Latitude–longitude distributions. For a more detailed study, using the MCMUA model, we calculated the longitude–latitude distributions of the hydrodynamic fields at given altitudes.

Figure 2 shows the longitude–latitude distributions of zonal wind and SOW amplitude in the troposphere for January. It can be seen from Fig. 2a that the troposphere has two eastward jet streams at mid-latitudes of the Northern and Southern hemispheres. The streams are inhomogeneous and have a velocity maximum of up to 50 m/s over the Atlantic and Pacific oceans in the Northern Hemisphere and over the Pacific and Indian oceans in the Southern Hemisphere. In the equatorial region, the zonal flows in Fig. 2a are westward. The model distribution of winds in Fig. 2a is very consistent with UK Met Office data. An analysis of the calculations for consecutive days showed that the zonal wind distributions are rather stable and similar to Fig. 2a in January–February.

This study takes the winds at small heights flowing around mountains and generating SOWs to be proportional to the MCMUA-model winds at an altitude of 7 km (see Fig. 2a); here, the proportionality coefficient decreases with a decrease in the effective height of the surface relief in each node of the horizontal grid of the model. Figure 2b shows for January 2005 the calculated latitude–longitude distribution of amplitudes of model-generated SOW velocity extrapolated

to a fixed height of 12 km. It can be seen that, in the Northern Hemisphere, the areas of increased SOW-velocity amplitudes are very consistent with the location of the major mountain ranges (the Himalayas, the Cordillera, the Rocky Mountains, Greenland, the Alps, the Caucasus, etc.). In the Southern Hemisphere (see Fig. 2b), the number of areas with increased SOW amplitudes is smaller than in the Northern Hemisphere, and they are located over the major mountain ranges of South America, Australia, Africa, and Antarctica. In January, the winds in the lower atmosphere are on average stronger in the Northern (winter) Hemisphere (see Fig. 2a). This also contributes to the generation of SOWs with amplitudes of up to 30 m/s in the Northern Hemisphere. As a result of this stability of zonal flows in the lower atmosphere in January–February, the distribution of areas with increased SOW amplitudes in Fig. 2b is also stable at that time.

Figure 2c shows the incremental velocities of zonal circulation in the troposphere in January, caused by the dynamical effects of SOWs. In most of the Southern Hemisphere in Fig. 2c, the absolute values of IVs are no more than 1 m/s due to the small number of areas of increased amplitudes of SOWs in Fig. 2b in the Southern Hemisphere. The greatest extremes of IVs in the Southern Hemisphere in Fig. 2c as found in South America near the area of maximums of SOW amplitudes in Fig. 2b over the Andes.

One interesting feature of this maximum is that it is distant from other areas of increased SOW amplitudes. An analysis of Fig. 2c shows that such an isolated maximum of SOW amplitudes creates an acceleration (positive IVs) of the zonal flow windward to the mountain system and deceleration (negative IVs) behind mountains in the troposphere at a latitude of around 30° S, near South America, where this maximum is located. Figure 2c also shows that the areas of positive and negative IVs are accompanied by areas of opposite signs north and south of the areas. Thus, the generation of SOWs over isolated mountain systems can create local circulation cells in the troposphere near a mountain barrier.

The Northern Hemisphere has more mountain ranges than the Southern Hemisphere, and Fig. 2b shows more areas with increased SOW amplitudes. Therefore, the circulation cells created by different mountain systems overlap one another and produce a complex system of adjacent areas of positive and negative IV values (up to $\pm 3\text{--}4$ m/s), which covers the entire Northern Hemisphere (Fig. 2c). Here, the areas of positive and negative IV values are shifted relative to mountain systems and can be located even over oceans.

Figure 3 is similar to Fig. 2 except for a height of 50 km in January. Figure 3a shows that there is an eastward jet stream in mid-latitudes of the Northern (winter) Hemisphere and a westward jet stream in mid-latitudes of the Southern (summer) Hemisphere. These

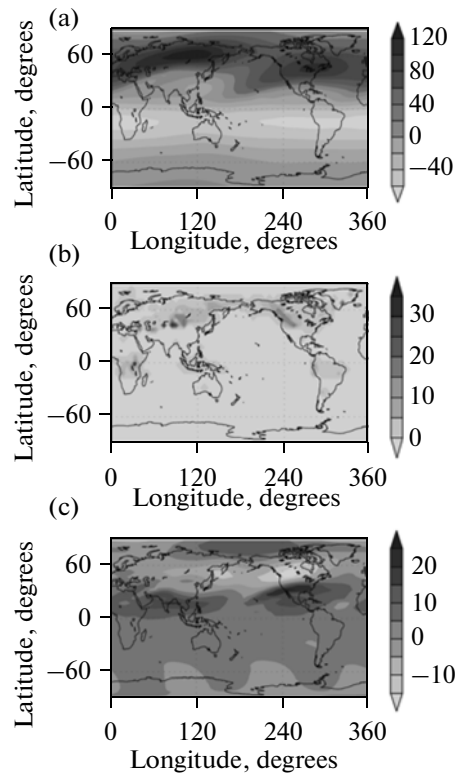


Fig. 3. Same as Fig. 2 except at an altitude of 50 km.

jet streams are inhomogeneous especially in the Northern Hemisphere, where two velocity maxima can be seen, which are apparently caused by planetary waves in the middle atmosphere (Fig. 3a). This distribution of winds remains stable during the calculations for January–February with slight velocity variations, such as those due to the influence of diurnal tides.

The distributions of SOW-velocity amplitudes in Fig. 3b for a height of 50 km show a small number of areas of increased amplitudes over the Southern Hemisphere. This is due to the above mentioned (see Fig. 1b) dissipation and filtration of SOWs near the critical levels generated by reversed circulation in the summer strato-mesosphere at mid-latitudes. The Northern Hemisphere has fewer tropospheric areas of increased amplitudes of SOWs in Fig. 3b than in Fig. 2b.

This is explained by the effect of mean wind velocity and temperature on the distribution of orographic gravity waves. In [9] it was shown that the energy exchange between a wave and mean flow, as well as the dissipation of wave energy due to molecular viscosity and heat conduction, may increase or decrease the amplitudes of SOWs with height. The remaining areas of increased amplitudes of SOWs in Fig. 3b are located (similar to Fig. 2b) over mountain systems, mainly in Central Asia and North America in the Northern Hemisphere. The amplitudes of SOWs in Fig. 3b on average increase in comparison with Fig. 2b. The location of areas of increased amplitudes of SOWs in Fig. 2b

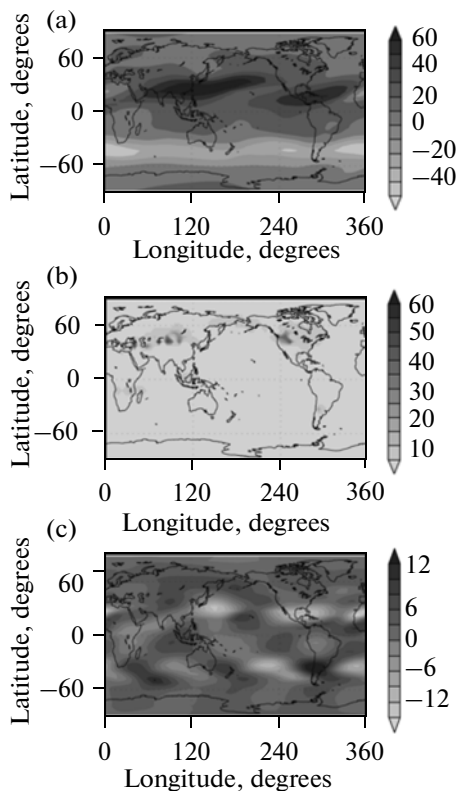


Fig. 4. Same as Fig. 2 except at an altitude of 80 km.

coincides with the latitude–longitude distribution of amplitudes of atmospheric waves with vertical lengths of 10–100 km for winter in the Northern Hemisphere at altitudes of 30–40 km according to microwave limb sounding data from UARS and Aura satellites [6, 7] and SABER infrared sounding instrument [21].

The incremental zonal velocity of circulation in Fig. 3c in the Southern Hemisphere is higher at low- and high-latitudes because the wind system in the stratosphere of mid-latitudes of the summer hemisphere contributes to a strong filtering of SOWs propagating from the troposphere. In the Northern Hemisphere, the reduced number of areas of increased amplitudes of SOWs in Fig. 3b leads to fewer extremes of IVs in Fig. 3c at an altitude of 50 km when compared with Fig. 2c for the troposphere. In Fig. 3c one can identify an area of negative IVs over the mountains of Central Asia with associate areas of positive IVs located north and south of the mountains. The interaction of these flows with the disturbances created by the mountain ranges of North America leads to the formation of a system over America that consists of two areas of positive IVs and two areas of negative IVs (see Fig. 3c).

Figure 4 corresponds to an altitude of 80 km in January of 2005. Similar to Fig. 3a for an altitude of 50 km, the average zonal wind in Fig. 4a has two jet streams: one eastward in the mid-latitudes of the

Northern (winter) Hemisphere and the other westward in mid-latitudes of the Southern (summer) Hemisphere. Figure 4b shows that the number and length of areas with increased amplitudes of SOWs at an altitude of 80 km are reduced when compared with Fig. 3b due to increased turbulent and molecular viscosity, heat conduction, and wave dissipation. In this case, the maximum amplitudes of SOWs are higher in Fig. 4b than in Fig. 3b, and they are higher in the Northern (winter) Hemisphere than in the Southern Hemisphere.

Due to the impact of SOWs, the incremental velocities of zonal circulation in Fig. 4c have the form of alternating areas of positive and negative IVs in both the Northern and Southern hemispheres. In the Southern (summer) Hemisphere, the maximal IV changes (within ± 10 m/s) occur in the area of the abovementioned jet stream at latitudes of 20° – 50° S. In Fig. 4c, the location of areas of positive and negative IVs in the Southern Hemisphere has a regular periodic form with three maxima and minima along the latitude circle, which look like planetary waves. In Fig. 4c, the main areas of extreme IVs in the Northern Hemisphere are also located at jet stream latitudes of 10° – 40° and have a periodic structure with three maxima and minima along the latitude circle. The maximum values of IVs in the Northern Hemisphere in Fig. 4c can reach up to 25–30% of the maximum circulation velocity in Fig. 4a.

Figures 2–4 show that the inhomogeneous distribution of mountain systems and tropospheric flows over the globe and the relevant inhomogeneous characteristics of generated SOWs can lead to significant changes in the general circulation of the middle and upper atmospheres. The change in tropospheric winds during the simulation on consecutive days leads to a shift in the areas of maxima and minima of IVs similar to Fig. 2c (both westward and eastward). The propagation of SOWs is affected by the distributions of the mean wind velocity and temperature in the whole atmospheric column. These distributions also vary during the experiment. Therefore, the velocities and limits of the shift of circulation disturbances increase with altitude. The analysis showed that the structures of major IV extremes for the simulation period of January–February are rather stable (Figs. 2c–4c). At the same time, the constant change in the mean wind velocity and temperature leads to the constant displacement of IV extremes, which resembles a planetary-scale wave propagation.

An analysis of distributions similar to Figs. 2–4 for July shows a stronger influence of SOWs on the circulation of the Southern Hemisphere, which is winter in this season and provides the best conditions for the propagation of SOWs (see Fig. 1). In the periods of solstices (April and October), the distributions of SOW characteristics and disturbances of atmospheric circulation induced by them are more homogeneous over the hemispheres.

In [23, 24], measurements of temperature disturbances in the mesosphere and lower thermosphere generated by orographic waves were performed for the regions of the Ural Mountains and over the Caucasus range. The results of numerical simulations described above show that the SOWs can create not only wave oscillations, but also temperature disturbances over large areas related to changes in the circulation due to the impact of wave accelerations and heat influxes. Therefore, the disturbances of atmospheric parameters associated with SOWs cover large areas and can be observed not only over mountain systems, but also in areas considerably far from the mountains.

5. CONCLUSIONS

Our parameterization of the dynamic and thermal effects of SOWs generated by the earth's surface topography [9] has been implemented in the numerical model of the general circulation of the middle and upper atmospheres. The potential changes in atmospheric circulation under variable conditions of the generation and propagation of SOWs in different seasons have been simulated.

The calculated values of wave heat influxes of up to 10 K/day and wave accelerations of up to 20 ms⁻¹/day at altitudes of around 50 km show that the orographic waves significantly affect the dynamic and thermal regimes of the middle atmosphere. In January and July, the main influence on the change in the zonal circulation velocity (up to 20 m/s) by orographic waves was observed in the Northern and Southern hemispheres, respectively. This can be explained by more favorable conditions for the propagation of SOWs in winter structures of background temperature and wind in comparison with summer structures. In equinox seasons, the distribution of orographic wave effects is more homogeneous in both hemispheres.

Thus, the horizontal inhomogeneities in the characteristics of SOWs can lead to the formation of quasi-stationary and moving inhomogeneities in hydrodynamic variables that can cover the entire atmosphere.

ACKNOWLEDGMENTS

This study was supported by the Russian Foundation for Basic Research, project nos. 10-05-00719, 11-05-00971 and 12-05-33071, as well as the Federal Agency of Education within the Federal Target Program "Scientific and Scientific-Pedagogical Personnel of an Innovative Russia" for 2009–2013, state contract no. P107.

REFERENCES

1. F. Lott and M. J. Miller, "A new subgrid-scale orographic drag parametrization: its formulation and testing," *Q. J. R. Meteorol. Soc.* **123** (537), 101–127 (1997).
2. S. B. Vosper and A. R. Brown, "The effect of small-scale hills on orographic drag," *Q. J. R. Meteorol. Soc.* **133** (627), 1345–1352 (2007).
3. J. F. Scinocca and N. A. McFarlane, "The parameterization of drag induced by stratified flow over anisotropic orography," *Q. J. R. Meteorol. Soc.* **126** (568), 2353–2393 (2000).
4. N. M. Gavrilov and S. Fukao, "A comparison of seasonal variations of gravity wave intensity observed with the middle and upper atmosphere radar with a theoretical model," *J. Atmos. Sci.* **56**, 3485–3494 (1999).
5. P. Preusse, A. Dornbrack, S. D. Eckermann, M. Riese, B. Schaeler, J. T. Bacmeister, D. Broutman, K. U. Grossman K. U., "Space-based measurements of stratospheric mountain waves by CRISTA: 1. Sensitivity, analysis method, and a case study," *J. Geophys. Res.* **107** (D23), 8178 (2002). doi 10.1029/2001JD000699
6. J. H. Jiang, D. L. Wu, S. D. Eckermann, and J. Ma, "Mountain waves in the middle atmosphere: microwave limb sounder observations and analyses," *Adv. Space Res.* **32** (5), 801–806 (2003).
7. D. L. Wu and S. D. Eckermann, "Global gravity wave variances from *Aura* MLS: Characteristics and interpretation," *J. Atmos. Sci.* **65** (24), 3695–3718 (2008). doi 10.1175/2008JAS2489.1
8. N. M. Gavrilov, "Structure of the mesoscale variability of the troposphere and stratosphere found from radio refraction measurements via CHAMP satellites," *Izv., Atmos. Ocean. Phys.* **43** (4), 451–460 (2007).
9. N. M. Gavrilov and A. V. Koval', "Parameterization of mesoscale stationary orographic wave forcing for use in numerical models of atmospheric dynamics," *Izv., Atmos. Ocean. Phys.* **49** (3), 244–251 (2013).
10. D. S. Phillips, "Analytical surface pressure and drag for linear hydrostatic flow over three-dimensional elliptical mountains," *J. Atmos. Sol.–Terr. Phys.* **41**, 1073–1084 (1984).
11. A. I. Pogoreltsev, A. A. Vlasov, K. Froehlich, and Ch. Jacobi, "Planetary waves in coupling the lower and upper atmosphere," *J. Atmos. Sol.–Terr. Phys.* **69**, 2083–2101 (2007). doi 10.1016/j.jastp.2007.05.014
12. A. I. Pogoreltsev, "Generation of normal atmospheric modes by stratospheric vacillations," *Izv., Atmos. Ocean. Phys.* **43** (4), 423–435 (2007).
13. K. Froehlich, A. Pogoreltsev, and Ch. Jacobi, "Numerical simulation of tides, Rossby and Kelvin waves with the COMMA-LIM model," *Adv. Space Res.* **32** (5), 863–868 (2003).
14. H. J. Jakobs, M. Bischof, A. Ebel, and P. Speth, "Simulation of gravity wave effects under solstice conditions using a 3D circulation model of the middle atmosphere," *J. Atmos. Terr. Phys.* **48**, 1203–1223 (1986).
15. N. M. Gavrilov, A. I. Pogoreltsev, and C. Jacobi, "Numerical modeling of the effect of latitude-inhomogeneous gravity waves on the circulation of the middle atmosphere," *Izv., Atmos. Ocean. Phys.* **41** (1), 9–18 (2005).
16. G. I. Marchuk, *Numerical Methods in Weather Forecast* (Gidrometeoizdat, Leningrad, 1967) [in Russian].
17. G. Strang, "On the construction and comparison of difference schemes," *SIAM J. Numer. Anal.* **5**, 516–517 (1968).

18. T. Matsuno, "Numerical integration of the primitive equations by a simulated backward difference method," *J. Meteorol. Soc. Jpn.* **44**, 76–84 (1966).
19. J. R. Holton, *The Dynamic Meteorology of the Stratosphere and Mesosphere*, Meteorological Monograph No. 37 (Am. Meteorol. Soc., 1975).
20. J. F. Scinocca and B. R. Sutherland, "Self-acceleration in the parameterization of orographic wave drag," *J. Atmos. Sci.* **67** (8), 2537–2546 (2010).
21. P. Preusse, S. D. Eckermann, M. Ern, J. Oberheide, R. H. Picard, R. G. Roble, M. Riese, J. M. Russell III, and M. G. Mlynczak, "Global ray tracing simulations of the SABER gravity wave climatology," *J. Geophys. Res.* **114**, D08126 (2009). doi 10.1029/2008JD011214
22. J. Gong, D. L. Wu, and S. D. Eckermann, "Gravity wave variances and propagation derived from AIRS radiances," *Atmos. Chem. Phys.* **12** (4), 1701–1720 (2012).
23. N. N. Shefov, N. N. Pertsev, M. V. Shagaev, and V. N. Yarov, "Orography-induced variations in the upper atmosphere emission," *Izv. Akad. Nauk SSSR, Fiz. Atmos. Okeana* **19** (9), 920–926 (1983).
24. V. A. Sukhodoev and V. N. Yarov, "Temperature variations of the mesopause in the leeward region of the Caucasus ridge," *Geomagn. Aeron.* **38** (4), 545–548 (1998).

Translated by V. Arutyunyan